 Bull. Chem. Soc. Jpn., 76, 891–902 (2003)

Theory of Molecular Excitons in 1-D Crystals as Applied to a Multiple-Helix Model of Pseudoisocyanine (PIC) J Aggregates[1]

Nobuaki Kanamaru

Department of Chemistry, Faculty of Science, Nagoya University, Furo-cho, Chikusa, Nagoya, Aichi 464-8602

(Received October 24, 2001)

The theory of molecular excitons in one-dimensional (1-D) crystals with 3-D entities is developed as a modification of the existent theory (for 3-D crystals), starting from a settlement of the 1-D space group. Then, it is applied to one of the helix models of the PIC J aggregates, as postulated, to interpret various experimental facts, such as the importance of hydrophobic groups and evidence of a core, i.e. a building block with (at least) 8 PIC molecules. Through the development of a formalism, the absorption and rotation of light by a helix with more than two spirals ($2 \times 4 = 8$ spirals corresponding to 4 double linear arrays, actually) are estimated and found to be consistent with the observed polarized absorption and circular dichroic spectra of the aggregates.

A general theory of excitons in (3-D) molecular crystals is well established, as demonstrated by a famous textbook by Davydov.[2] However, few comprehensive papers have appeared which describe 1-D exciton in general in a form comparable to those of 3-D exciton, as may be seen in a review paper by Philpott.[3] One of the reasons may be traced to a scarce demand for its establishment. Actually, the theory of circular dichroism (CD) for the 1-D system published so far is only concerned with polymers with less than three spirals,[3–5] to which the present multiple-helix models do not belong. Therefore, one of the purposes of this paper is to build up a (numerically tractable) formalism for 1-D exciton by taking the PIC J aggregate as the first example.

1,1′-Diethyl-2,2′-(quino)cyanine, frequently referred to as pseudoisocyanine (PIC), is a dye cation with a nonplanar conformation composed of planar 1,2-dihydro-1-ethylquinolin-2-ylidene and $1^{(\prime)}$-ethylquinolinium (π) groups attached on a methine (CH) group at their $2^{(\prime)}$ positions (the cut in Fig. 1). As evident from its resonance structures, PIC shows a strong absorption band in the visible region, whose 0,0 band is located at ~525 nm, e.g. in a diluted aqueous solution. On the other hand, its J aggregate (a classical system of self-assembling) is formed in highly concentrated solutions exhibiting a sharp red-shifted J band at ~575 nm (~17400 cm^{-1}), in addition to two H bands (the notation in this paper, not always applied to other papers) at ~505 nm that are retained even after completion of aggregation, and finally reaching ~530 (~18900) and ~490 (~20400) nm (cm^{-1}). These are parallel and perpendicular to the growth axis of the aggregate, respectively. Since the earliest discovery by Scheibe[6] and Jelly,[7] the title system has been one of the most frequently studied typical J aggregates of huge size (consist of ~(>)100 monomers), but with peculiar characteristics, even in solutions.[8–39] (1) Besides a sharp red-shifted J band, it shows at least two more H bands at shorter wavelengths with 50% more intensity put together (for chloride: PIC-Cl). (2) The polarizations of the J and H bands are parallel and perpendicular to the growth axis of the aggregate, respectively. (3) It has chirality, as evidenced by the CD in the presence of optically-active counter anions, with opposite signs between the J and H-band areas. Though various structures have been proposed, none of them can fully interpret the above facts.[25] (Ref. 18 appears to be the only paper that claims to have interpreted the above three criteria. However, the double linear (DL) array, as proposed in Ref. 17, is widely used in the current literature, which took over the previously dominated brickwork model,[28] both as clippings from the crystal. In this respect, Fig. 6 in Ref. 40 may be the best illustration of the DL array, though a greatly simplified version, as expressed by the two lines of the bricks, is of common use. Of course, this figure is an extract from a particular crystal of PIC-I.[40] Thus, we can imagine various types of DL arrays in solution by changing the fine details, like those in Refs. 12, 17, and 28. For example, a model calculation[25] with a point-dipole approximation on all of the possible parallelogramic planar $2 \times 16 = 32$-mer (i.e., the brickwork product consist of 16 dimers with partial overlap between the π planes of the monomers) ranging

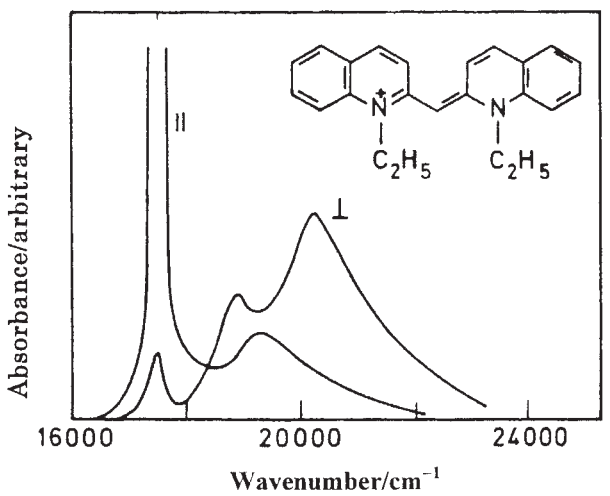

Fig. 1. Polarized absorption spectra of a highly concentrated aqueous solution of PIC.[10,17]

from a zigzag ladder-type (16×2) aggregate to a staircase-type (1×32) aggregate with a gentle inclination (slipped single linear array?), through a 2×16 DL array, failed to interpret the polarized absorption spectra.[10,12,28] Therefore, the coexistence of 16×2 and 1×32 types as ca. 1:1 mixture had to be presumed in the stream.[25] (Very recently, a similar idea concerning coexistence was proposed based on a theory with a CES approximation.[39]) Most significantly, to interpret the ratio (ca. 1:1.5) of the integrated intensities between the $\parallel$ and $\perp$ bands (that may be a zeroth-order representation of the intensity ratio between the J and H bands) assuming a (double) linear aggregate with two PIC molecules in the unit cell, the angle between the transition moments of two adjacent molecules had to be assumed at $\sim 70^\circ$, while ascribing one of the two H bands to the vibronic band (e.g., assisted by the nonadiabaticity operator).[17,18,30,33,34] This is hardly acceptable for the intermolecular arrangement picked up from those in crystals, where the angle made with their molecular long axes never exceeds 30° for any pair of adjacent PIC molecules, whose π planes of aromatic rings are in partial contact with each other.[40–42] As pointed out by the present author,[25] this fact has not been recognized by the researchers in this field, as evidenced e.g., with the illustrations of the DL arrays, even in current publications, such as Ref. 27, with the exceptions, e.g. of Refs. 33 and 34. (A zigzag model as proposed in a latest paper,[38] appears to be very close to that in these papers.) Therefore, the title structure to be described in this paper may be regarded as being the first one that can interpret all of the experimental data more than sixty years after discovery.

In Section 1, the PIC systems are reviewed. A presentation of the helix structure is made in the next Section 2, which is followed by a general theory of molecular excitons in 1-D crystals. Then, in Section 4, the actual procedure is taken to acquire the wavefunctions and energies of the exciton states and to make assignments of the absorption and CD spectra in the PIC J aggregate with the $D_2{}^1$ symmetry of 1-D space groups (SGs). (This transaction should easily be extended to any other systems of any different 1-D SGs.) The predominance of the present model over others is evident just by recognizing the clearer reproduction of the intensity distribution among the polarized bands than the previous ones. Namely, the spectra in Fig. 1 are what should be interpreted first concerning characteristics (1) and (2). (Besides the major three bands, i.e. one sharp $\parallel$ J and two broad $\perp$ H bands, a weak $\parallel$ band at $\sim$520 nm ($\sim$19200 cm^{-1}) is also noticeable, with no nickname, due to a lack of popularity, that cannot be interpreted as being due to incomplete alignment in the stream. This is a subject for a future publication to present a more quantitative discussion.[43]) The present figure is just used to reproduce Fig. 1 of Ref. 17 with modifications which, itself, is taken from Ref. 10 as the spectra of the streaming aqueous solution of PIC. With an alternate interpretation of this data, i.e. with a more realistic structural model, the present theory may be regarded as being a sublation of their theories.[17,18] Similar polarized spectra are also reported in recent publications for spin-coated PVA solutions of PIC-Br.[26,29] In Section 5 of Concluding Remarks, an interpretation of more data is made in a less quantitative manner, in addition to a general conclusion.

1. Critical Review

An enormous number of papers ($\gg$100 ?) have been published on PIC systems, probably because they form huge J aggregates under various conditions. However, a review will be made mainly concerning the PIC J aggregate in solution (at room temperature).

1.1 Initial Stage of Aggregation before the Formation of the J Aggregate. Cooper[11] observed the temperature effect of the absorption spectrum of 4×10^{-4} M EG-W (1:1 ethylene glycol–water) solution of PIC-Br: At room temperature (298 K), it shows a monomer spectrum with the most intense maximum at 525 nm. However, at 173 K, a new band appears centered at 483 nm, accompanied by an (apparent) decrease in the monomer-band intensity by half. Since it is blue-shifted from the monomer band, the new band was ascribed to a ''dimer'' with an H-type (parallel) conformation.

Kopainsky et al.[15] succeeded to cleanly separate the ''first'' step of aggregation of PIC-Cl in the aqueous solution by observing the absorption spectrum without the J band under various conditions, and in drawing out a ''dimer'' spectrum by a simulation. Contrary to the conclusion by Cooper,[11] the dimer spectrum has double peaks at 481 and 522 nm. However, two questions arises from both experimental and theoretical aspects:[25] (1) Regarding the former, the invalidity of the law of mass reaction, as mentioned by the authors, themselves, must be investigated. Actually, a trial to fit their data by the present author, assuming the equilibrium of either

$$n\mathrm{M}^+ = (\mathrm{M}^+)_n \tag{1a}$$

or

$$n\mathrm{M}^+ + n\mathrm{X}^- = (\mathrm{M}^+\mathrm{X}^-)_n, \tag{1b}$$

was a failure for any n ($= 2, 4, 8$), with M^+ and X^- indicating the PIC cation and halide anion (X = Cl, actually), respectively. (Their concern appeared to be Eq. 1a with $n = 2$. However, they didn't add salts, such as NaCl, to adjust the ionic strength of Cl^-.) This fact points out any puzzle in the data analysis, such as the involvement of more than two kinds of species. Recently,[37] based on a static light-scattering experiment, Neumann estimated the aggregation number of the ''dimer'' to be 4–30, depending on the ionic strength. (2) Another question concerns the assignment of the dimer spectrum by invoking a vibronic coupling theory with a nonadiabaticity operator (their Appendix) using a ''dimer'' model (their Fig. 3). Actually, the angle $\alpha \approx 70^\circ$ required to interpret the intensity ratio for $|\boldsymbol{M}_\mathrm{A} \pm \boldsymbol{M}_\mathrm{B}|^2/2 = M^2(1 \pm \cos\alpha)$ is too big compared to that in a crystal, if the transition moments in individual PIC molecules ($\boldsymbol{M}_\mathrm{A}$, $\boldsymbol{M}_\mathrm{B}$) are assumed to be along the molecular long axes. This criticism is just applied to Refs. 17 and 18, where this dimer model is used as a unit cell for their 1-D J aggregates, as well as to Refs. 33 and 34, all four requiring the intensity mixing mechanisms to produce double H bands (if no progression is assumed as a common habit for large aggregates), as already unveiled in Introduction.

1.2 The Peculiarities of the PIC J Aggregates. Reference 12 may be regarded to be one of the best review papers (at the time when it was published). There, all the three criteria, (1)–(3), as described in Introduction, are already mentioned. Be-

sides these, following facts are noted: (4) Evidence for formation of aggregation nuclei (coexistent with the J aggregate) which may correspond to Eq. 1b with the observed minimum association number $n = 8$, and (5) which may be associated with the importance of hydrophobic groups. (6) A gradual change of the spectral shape with the progression of the association, especially near the H bands, while increasing the relative contribution of the J band. Namely, the shape and the intensity (distribution) of the H bands (compared to the J band) are dependent on the size of the aggregate. (7) Complex and strong dependencies on the choice of counter-anions, and many other facts.

As for the ultimate intensity ratio (ca. 1:1.5) between the J and H bands, the environmental effects should be mentioned as follows: (1) If J aggregates are formed in (2-D) monolayers, the contributions of the H bands are much less (at one order of magnitude) than those of the J bands, just in conformity with the prototypical J aggregates.[19–21,24] Namely, the formation of 3-D structures seems to be a prerequisite for the appearance of the H bands.[25] In contrast, (2) the absorption spectrum of the J aggregate, especially with the counter anion (I^-) in EG-W at 4.2 K shows rather enhanced H bands (nearly one order-of-magnitude larger than the J band, probably beyond the experimental artifact, e.g. to reduce the intensity of the J band, Fig. 3 of Ref. 23) that may be ascribed to the solvent-cage effect.[25,32]

Finally, evidence of two kinds of J aggregates should be noted, i.e. with two origins of the J-band separated at $\sim$180 cm^{-1}, as found in rigid solutions of PIC-X (X = Cl, Br, I) at low temperatures.[11,22–24] Their intensity ratio is found to be dependent on the choice of the counter halide ion. The larger is the ionic radius, the larger is the contribution of the red form. As described above, a similar tendency should be noted concerning the H/J intensity ratio (cf. Fig. 1 of Ref. 24). In short, with a halide ion of larger ionic radius, the red form is more populated, probably accompanied by a higher intensity of the H bands.

All of the above and several other facts (mentioned in the next Section) are what must be interpreted. However, the entire structure model so far proposed was merely a partial success.

2. The Helix Structure of the PIC J Aggregates

The present multiple-helix structure assumes a pillar composed of 4 or 6 DL arrays (winding it as 8 or 12 spirals) that are akin to, but different from, those found in crystals.[40–42] Namely, it may be viewed as a cord made of (4 or 6) strings of DL arrays. Like crystals, this helix accommodates both J- and H-type arrangements in 2-D. To say precisely, they are spirals of the DL array and the rolled zigzag ladder-type aggregate (at the same time) and wind the pillar (themselves, to say precisely) obliquely and vertically (to the growth axis), respectively. Contrary to that in a crystal where the pointing directions of the ethyl groups or sides of the central C atoms are alternated in the array,[40–42] however, the entire hydrophobic ethyl group is packed in the core of the column. (Though the importance of the hydrophobic groups for the formation of the J aggregate had been noted from long time ago,[12] no model structure with a distinct hydrophobic interaction like this has been proposed.) While the counter anion is expelled just outside of the pillar to compensate for the plus charge of the PIC cation, and is hydrogen-bonded with the cluster of solvent molecules, $(H_2O)_n$. Therefore, this can be regarded as a sort of rod-type micelle with an extremely small diameter (a kind of small-sized nanomaterial, i.e. mesoscopic system), smaller than what are described in Ref. 27.[7,12]

Figure 2 is drawn to illustrate a schematic structure based on the above assertion for the case of a particular enantiomer with four DL arrays. Among various alternatives, one of the conceivable structures, as examined starting from the highest possible symmetry, was picked up while manipulating a set of molecular models composed of atoms scaled with van-der-Waals radii (as will be shown later) and consulting (stereo views of) the crystalline data.[40–42] A detailed description of the consequence of the manipulation procedure, i.e. a sort of experiment, is described in the figure caption. Here, it should be emphasized that the figure is a spread view of the cylinder (seen from outside) with symbolical representations of projected images of the 3-D entities (on the surface). (Keen imagination, hopefully with a pair of molecular models, may be requested to understand the adequacy of the complex structure of this kind.)

Now, let's start constructing the J aggregate by assembling molecular models of PIC. First of all, a trial, i.e. an initially-chosen structure with the highest site symmetry (symmetry of the local arrangement without taking account of the whole environment), i.e. the primary version of Fig. 2, is characterized. Instead of 4 DL arrays, it consists of (1) octal helix of 8 single linear arrays with equidistant separations from the adjacent ones, where all of the PIC molecules form a face-to-face (full π) pair with a molecule in the adjacent array interchangeable by a C_2 symmetry operation, like a $\boldsymbol{B}^{\beta}_{m,n} - \boldsymbol{A}^{\beta}_{m,n}$ pair in Fig. 2 (but with a closer distance between them and with much less contact between their ethyl groups than in this figure). In this respect, this may also be regarded as 4 DL arrays whose forms are quite different from the customarily presumed structures, i.e. with no distinct attractive force to hold themselves along the straight growth lines of the spirals and each of which (2) consists of only one kind of PIC enantiomer. However, the helix as a whole is presumed to be composed of a 1:1 mixture of PIC enantiomers (with alternation in every two spirals) both with (3) C_2 symmetries of molecular point group (MPG). (4) The inclination angle of the DL array (γ), to represent one of the parameters for the primitive lattice (vide infra), is defined as $\pi/4$ so as to secure the highest local/site symmetry of the PIC molecules (if spread). At this stage, it is worthwhile to note that an alternative/equivalent definition of $\gamma' = 3\pi/4$ is also possible, in accord with the symmetry. Thus, the choice of $\gamma = \pi/4$ was made just to conform with the inner structure (the orientation of the arrays) of the present enantiomer of the helix. However, this structure is not tight enough to form a rigid structure, due to the weak π interaction between aromatic planes to hold each array along its growth line, barely supported by the attractive force of the counter anion in addition to the hydrophobic force. (A theoretical calculation of the exciton states for this geometry, with the procedure, as described in Section 4, was also a failure for interpreting the observed absorption spectra just as the case of the planar 32-mers, as mentioned in Introduction.)

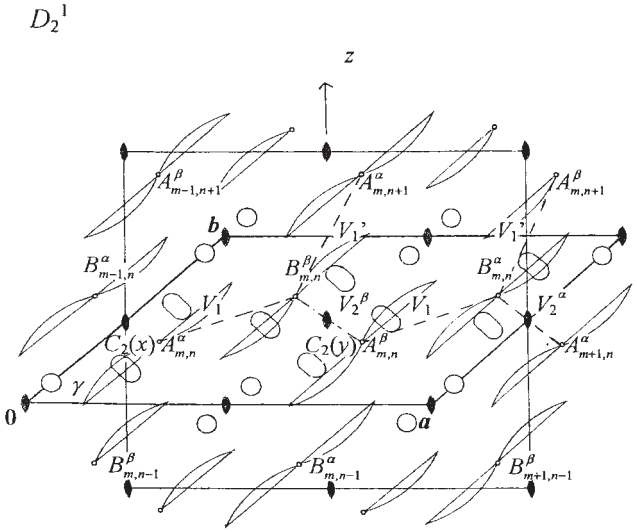

Fig. 2. Projected/spread view of (a front half of) a helix with four double linear (DL) arrays in the PIC J aggregate. One of the enantiomers with clockwise spirals was picked up arbitrarily. The central C atom of the nonplanar PIC molecule, as indicated by $X^{\xi}_{m,n}$ and sketched symbolically by the double bow to indicate upwardly-open pairs of aromatic groups/planes, is just working as a joint of the strings to represent the backbone of PIC, to which elongated circles to designate the expelled ethyl groups are attached (drawn only for the smallest possible "unit cell"; while circles denoting counter halide ions). The C atom is also located near the inside surface of the cylinder with a thickness of ~0.4 nm, whose average radius is ~0.9 nm. (Actually, the figure is a projection on this cylinder as spread, to which the average plane of all of the PIC molecules is assumed to be vertical.) Here, the indices run as follows: $\{X\} = (A, B)$, $\{\xi\} = (\alpha, \beta)$, $\{m\} = (1, 2)$, and $\{n\} = (1, 2, \cdots, N)$. The periodic boundary conditions are set and assumed for the latter two numbers, m and n, respectively. The symbols A and B are chosen to indicate an 8-membered slanted zigzag-type ring or crown with a common subscript number, n. α and β are to distinguish chiral stereomers of the PIC molecule, itself. The set of numbers (m, n) is to enumerate the primitive unit lattice judged to be suitable for representing the present 1-D crystal with the 1-D SG, $D_2{}^1$. For better 3-D imagination of this crystal, to pile up slices of Baumkuchen (annual-ring cake) may be appropriate, each of which is unusually cut into two pieces. (The inside cavity of the pile is filled with a jam made of ethyl groups, while the outside is decorated with counter halide anions, like rivets.) The definitions of $\mathbf{0}, \boldsymbol{a}$ ($a = \sim 2.8$ nm), $\boldsymbol{b}$ ($b = \sim 1.8$ nm), and γ ($= \sim 38°$) for the "unit cell" are easily discernible from the projected/spread figure with $a \approx 2b\cos\gamma$. The z axis runs through the center of the column, while the x and y axes cannot be set uniquely, merely being applied to an arbitrary ring, i.e. to the n-th disk as indicated by $C_2(x)$ and $C_2(y)$. (To say precisely, the number n matches with the times of a screw operation as a combination of a approximate $C_4(z)$ operation and a translation along z with a distance of $b\sin\gamma$.)

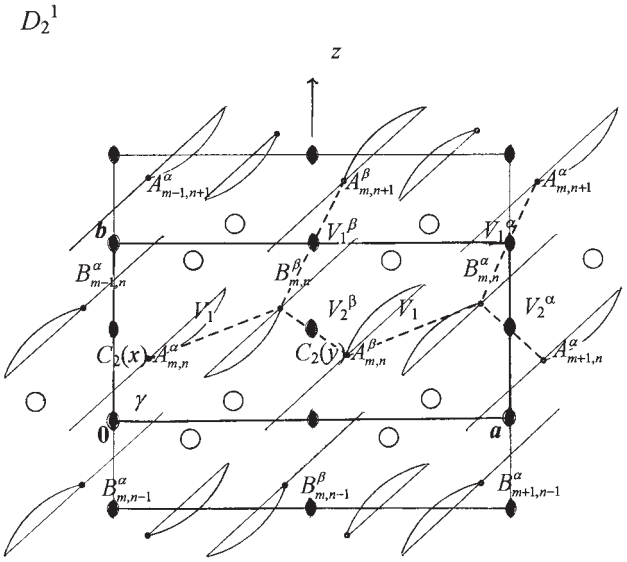

Fig. 3. Projected/spread view of the helix with four DL arrays in the PIC-F J aggregate. This is drawn so as to be just comparable to the preceding in Fig. 2. Instead of the double bow in the Fig. 2, the nonplanar PIC molecule is sketched symbolically by a spoon, whose short axis is no longer vertical to the pillar. The central C atom is indicated by $X^{\xi}_{m,n}$, just as in the previous case. However, the locations of the expelled ethyl groups are not indicated, bearing in mind the delicate dependence on such as the $X^{\xi}_{m,n}$ values in the present case. (The small circles are retained to denote the counter halide ions.) The C atom is also located near the inside surface of the cylinder with a thickness of ~0.4 nm, whose average radius is ~0.9 nm. Here, the indices run as follows: $\{X\} = (A, B)$, $\{\xi\} = (\alpha, \beta)$, $\{m\} = (1, 2)$, and $\{n\} = (1, 2, \ldots, N)$. The periodic boundary conditions are set and assumed for the latter two numbers of m and n, respectively. Just as in the Fig. 2, A and B are chosen to indicate the 8-membered slanted zigzag-type ring or crown with a common subscript, n. However, their geometries are different from each other in spite of the common arrangements. This is due to the different way of packing, as confirmed by the set of molecular models. On the other hand, α and β are used to distinguish chiral stereomers of the PIC molecule, itself. The set of numbers (m, n) is used to enumerate the primitive unit lattice judged to be suitable for representing the present 1-D crystal with the 1-D SG, $D_2{}^1$. The definitions of $\mathbf{0}, \boldsymbol{a}$ ($a = \sim 2.8$ nm), $\boldsymbol{b}$ ($b = \sim 1.25$ nm), and γ ($= \sim 90°$) for the "unit cell" (not for the DL array) are easily discernible from the projected/spread figure. The z axis runs through the center of the column, while the x and y axes cannot be set uniquely, merely being applied to an arbitrary ring, i.e. to the n-th disk, as indicated by $C_2(x)$ and $C_2(y)$.

Accordingly, it was admitted to deform by letting the PIC molecules shift their positions to assemble (1) the constituent DL array that consists of (2) 1:1 enantiomers of PIC molecules where ethyl groups at the one side of the array are expelled just outside of the contact pair composed of the parallel (half) π planes, like a $\boldsymbol{A}^{\alpha}_{m,n} - \boldsymbol{B}^{\beta}_{m,n}$ pair in the Fig. 2, while lowering

their own (3) local symmetry (including the environment) to C_1 (MPG, not of C_2, even excluding the environment actually; section 4.3) with (4) the reduced inclination angle, γ. (The Illustration in the Contents of this issue is an intermediate between the primary and the final versions for the Fig. 2.) Nevertheless, its symmetry as a whole, i.e. on SG, can always be kept with the initial one ($D_2{}^1$, the next paragraph). The average plane of all PIC molecules is also assumed to be vertical to the pillar (its short axis passing through the z axis vertically), as can be confirmed to be acceptable by molecular models. With the success of this model structure, we'll realize "How ingeniously the PIC molecule is designed to form the most typical, peculiar, and huge J aggregates!" For example, nonplanarity is the most important factor for the peculiarity of this molecule, i.e. for a feasible formation of the spiral.

A similar prescription is applied in choosing the unit cell, depending on the various ways to define it,[44,45] particularly for the 1-D crystal. Thus, the simplest possible one, i.e. the primitive lattice, is first selected (vide infra, apparent unit cell of half size in case of Fig. 2). The 8-membered disk just corresponds to the observed minimum association number of the PIC molecules (coexistent with the J aggregate), and may be taken as a core toward formation of the J aggregate.[12] (So far, no model structure of the J aggregate has been proposed that denotes a distinct structure consisting of 8-membered cores like this.) If we do not distinguish the possible conformers involving the ethyl groups (e.g., by assuming free rotation of the methyl (or ethyl) groups), all of the PIC molecules can be thought to be at equivalent positions, α and β being physically equivalent (but not completely after being wound in a helix; vide infra). By inspecting this figure, the symmetry of this 1-D crystal is judged to be $D_2{}^1$ (vide infra). Thence, the conventional theory of molecular exciton[2] is now applicable to the present system if some cautions are paid.

At this stage, other helix models of the PIC J aggregate, as were found in the literature, should be mentioned. Mason[9] proposed a helix with eight monomers per turn and a rise of ~0.45 nm per monomer along the helix axis, probably with the shape of a spring (like that of a shock absorber). This is a re-interpretation of the conclusion derived from an X-ray diffraction study (of PIC-F: Failure in determining any lattice constant for PIC-X with X $\neq$ F is apparently correlated with the experimental detection of the two conformers, as described in the preceding Section 1.) by Hoppe:[8] a thread-like polymer with a unit cell containing eight dye molecules repeating every 3.55 nm along the fiber axis. (The coincidence of this value of the unit lattice with twice the unit translation (b) in this paper should be noted, as will be interpreted in a future publication by a further refinement of the structure (of PIC-F).[43]) Nordén[14] proposed a coiled-band model consisting of such as a triple linear array apparently composed of bent types of brickwork models[13,28] (Fig. 7 of Ref. 14; with the appearance of a hose, whose inner diameter is measured to be ~4 nm, i.e. containing the media molecules inside while embedded in the media) to improve the above model. A helical aggregate proposed by Knapp et al.[18] (with the appearance of a stretched single spiral or spring) is quite different from the above models, and is composed of a dimer with the structure proposed by Kopainsky et al.,[15] as already mentioned. Though all of these can explain the chirality, they do not explain all aspects, as described above, including more than three criteria, as can be seen through the arguments in the succeeding Sections.

3. Theory of Molecular Excitons in 1-D Crystals

This Section is concerned with the title subject as a modification of that developed for 3-D molecular crystals.[2] It is further divided into three sections of SGs, excitons, and spectroscopy, all concerning 1-D crystals.

3.1 SGs for 1-D Crystals. First of all, it has to be emphasized that the SGs under consideration are not those described in the official handbook:[44] the 2 line groups, 17 plane groups, and 230 (3-D) SGs. Namely, what is considered here is the 1-D crystal with 3-D entity. With no official paper, the present author attained the following list of 1-D SGs:

$$pn(C_n{}^1), n = 1\text{–}\infty;; \quad pn/2(D_n{}^1), n = 1\text{–}\infty;;$$
$$pnm(C_{nv}{}^1), n = 1\text{–}\infty; \quad png(C_{nv}{}^2), n = 1\text{–}\infty;$$
$$cnm(C_{nv}{}^3), n = 1\text{–}\infty;; \quad pn/m(C_{nh}{}^1), n = 1\text{–}\infty\,(C_{1h}{}^1 = C_s{}^1);$$
$$cn/m(C_{2nh}{}^2), n = 1\text{–}\infty;; \quad p\bar{n}(S_{2n}{}^1), n = 1\text{–}\infty\,(S_2{}^1 = C_i{}^1);;$$
$$pnm/m(D_{nh}{}^1), n = 1\text{–}\infty; \quad png/m(D_{nh}{}^2), n = 1\text{–}\infty;$$
$$p\bar{n}m/m(D_{2nh}{}^3), n = 1\text{–}\infty; \quad cnm/m(D_{nh}{}^4); n = 1\text{–}\infty;;$$
$$p\bar{n}m(D_{2nd}{}^1), n = 1\text{–}\infty.$$

It should be noted that the point groups corresponding to these, i.e. those without superscripts, 1–4 (e.g., D_1) do not always exist in spite of more severe restriction for the symmetry operation in 1-D SG than that in MPG. Also, the line groups, i.e. $p1$ ($C_{\infty v}{}^1$) and pm ($D_{\infty h}{}^1$), are observed to be the limiting cases for $n \to \infty$ in the above list. To comprehend these SGs, the tables of line groups, plane groups, as well as point groups should be consulted. Actually, these groups are imagined through projections of the realities onto the cylinder (or the line). The definition of the crystal point group (CPG) in the 1-D crystal can be made just as in the 3-D crystal. Therefore, its symmetry operations can be picked up from those of the corresponding MPG. Thus, 13 kinds of 1-D SGs (slightly less than the number of the plane groups, vide infra) are counted, though the actual number is infinity, like that of the MPG. Now, the SG of the PIC J aggregate is judged to be $D_n{}^1$ with $n = 2$ or 3, as picked up from the above list (Section 4), superscript 1 indicating to be symmorphic.[44,45]

The peculiarities of the SG in the 1-D crystal (referred to the other cases such as the 3-D crystal) are stated/postulated as follows:

Ⅰ The 1-D crystal can always be regarded as a column that consists of disks as unit cells piled vertically, i.e. stacked horizontally with regards to z representing the principal/growth axis.

Ⅱ The actual shape of the disk need not be a true/round disk, i.e. it may contain an empty area, the symmetry of which may be as high as that admitted by the MPG.

Ⅲ However, the local symmetry of the disk (the unit cell), i.e. its CPG (that takes account of the environment) may not be very high, as exemplified here: Ⅲa The $C_n(z)$ operation may exist for any n (= 2–∞). Ⅲb The other C_n operation cannot exist for $n > 2$, i.e. except for the C_2 operation, whose axis crosses the z-axis vertically.

Ⅳ Only one freedom of a proper translation operation is available, which may not be a pure translation along z (applicable for $C_n{}^1$ and $D_n{}^1$ cases only, actually). Namely, a screw operation could be predominant over the pure/vertical translation. In the extreme case where a pure translation is not available as a symmetry operation, the screw operation is designated as being incommensurate. This might actually be the case for the PIC J aggregate. (The screw operation in the Fig. 2 does not necessarily consist of the $C_4(z)$ operation; namely, $a \equiv 2b\cos\gamma$ is applied only for the primary highest local/site symmetry (Section 2).)

To comprehend the above statements, the numeration of MPGs of a cylinder of finite length, i.e. with finite N, would be helpful. An (evenly) slipped stack of coins (that may not look like a cylinder) might appear to be incompatible with the above postulates (e.g., statement Ⅰ). However, by recasting, you can always find a new set of coins with unusual shapes (statement Ⅱ), to identify the SG.

With the above set of statements/postulates, to count out the 1-D SGs is now straightforward. First, one of the translation operations for the corresponding plane group is regarded as a $C_n(z)$ operation in the 1-D SG. Then, the remained translation for the plane group is recognized to be either a translation or a screw operation along z for the 1-D crystal, depending on the angle (γ, whether $= \pi/2$ or not) in its unit cell (i.e., primitive lattice). In this way, 13 ($= 5 + 4 \times 2$) kinds of 1-D SGs are numerated corresponding to 9 plane groups of either 2 oblique or 7 rectangular forms, with no correspondence to 8 other plane groups of either 3 square or 5 hexagonal forms.

Finally, a practical aspect in determining the SG of a given 1-D crystal is described. It concerns the corresponding plane group, projection on the cylinder being presumed. Thus, a 2-D primitive lattice at first should be sought that may be treated as a sort of ''unit cell'', if the projected/spread figure on the cylinder is regarded as a 2-D crystal with real/short and conventional/artificial/long periodic boundary conditions. (The 2-D crystal of this kind can be rolled into a 1-D crystal.) Thus, all of the possible 1-D crystal can be assigned to one of the SG in the above list. Actually, Fig. 2 (for the present system) is visualized based on this concept.

After this work on SGs was nearly completed, the author found two textbooks[46,47] that contain description of 1-D SGs.; the original versions of the both were written in Russian. Therefore, a comparison should be made among these: Shubnikov and Koptsik listed 19 types of symmetry for rods (with finite translations) in Table 5 of Ref. 46, while Vainshtein listed 15 families of cylindrical groups ($G_1{}^3$) and their radial projections in Table 2.9 and Fig. 2.59, respectively, of Ref. 47. (Four lens-shaped symbols for the C_2 axes are missing in one of their figures, i.e. that for $s_M N/2$ ($M = 3$), which is closest to the present Fig. 2 and belongs to a commensurate case in the family of symmetry groups $D_n{}^1$.) They are defined with quite different notations from each other, and are not very compatible with mine, i.e. with those given in International Tables.[44] Furthermore, the discrepancy among the numbers (13 kinds for the 1-D SGs, 19 types for rod, and 15 families for cylinder) should be noted. However, a close examination of these data elucidated one-to-one-to-one correspondences for the 11 classes, i.e. except for the two cases of $C_n{}^1$ and $D_n{}^1$, in this notation. Namely, each of these exceptional cases is in one-to-four and one-to-two correspondences with the other two sets of cases, respectively. This is intimately related to the attitudes in defining the SG, e.g. how to treat the two symmetry operations (screw vs translation) for these 2 (, 4, or 8) cases. At this stage, statement Ⅳ in this section 3.1 is highlighted (to dismiss the pure translation, occasionally), so that the incommensurate case is naturally introduced in contrast to the other two notations, i.e. the implicit definitions made in analogy to the simpler cases in Refs. 46 and 47 (such as a border symmetry group[47]). (Also, enantiomers are not clearly distinguished in this definition, but are rather represented, e.g. by the sign of $\pi/2 - \gamma$ for the present case.) Though their notations/definitions may be more suitable for describing the site symmetry while disregarding the environment (Section 4) (as is necessary for Art, but not giving rise to any other independent symmetry operation than those corresponding to the present form of SG), they are not adequately applied to describing the SG (in Science, e.g. the molecular exciton state characterized with the present form of 1-D SG). For example, there is no a priori (chemical) reason to expand the size of the unit cell (or of the primitive lattice) into twice, as indicated by the (near) rectangle (with twice the area of the parallelogram) in the Fig. 2. Actually, as described in the next Section, the character table for $D_2{}^1$ gives sufficient information to determine the full eigenfunctions of the present exciton system.

3.2 Molecular Excitons in 1-D Crystals. Not much discussion is given in this section, owing to the availability of excellent review papers.[2,3] Here, the peculiarity in the 1-D crystal is only mentioned as concerning the choice of the ''unit cell'' (Section 1). Namely, it may consist of several primitive lattices that are more tractable in the actual procedures, as in the next Section for the PIC J aggregate.

3.3 Absorption and Rotation of Light by the 1-D Crystals. Just as above, the peculiarity in the 1-D crystal is seen for the case where the crystal is composed of a helix, i.e. where a screw operation (if not predominant over translation) is involved. In this case, special care must be paid in evaluating the polarization spectra as well as the CD spectra, as can be seen by following the actual application procedures.

4. The Formalism as Applied to the PIC J Aggregate

Now, the theory of molecular exciton states is formally applied to the title system with the distinct structure shown in Fig. 2, whose symmetry is presumed to be one of the highest possible, i.e. $D_2{}^1$ in 1-D SG as picked up from the list in section 3.1. (The $D_3{}^1$ case will be discussed in a later paper.[43]) Therefore, the following procedure, i.e. the derivation of the following equations, is straightforward in accord with the prescription in a textbook,[2] if apprehension is paid to such as Eq. 2 with a generalized coordinate and to the last 12 Eqs. 16–24, peculiar to the 1-D crystal.

4.1 Zeroth-order Basis Functions. By consulting Fig. 2 showing spread view, including its caption, the basis function in conformity with the translational symmetry (of the screw operation involving the approximate $C_4(z)$ operation: The expression is applied for a generalized coordinate b as indicated in the spread view.) is given by

$$|k\rangle_{X(m,\xi)} = N^{-1/2}\sum_{n=1}^{N}|X^{\xi}_{m,n}\rangle \exp(ikbn) \tag{2a}$$

for the site $X(m,\xi)$ (in the disk) and the k value, which is restricted by the integer ν to satisfy

$$-N/2 < (Nkb/2\pi) \equiv \nu \leq N/2. \tag{2b}$$

Here, $|X^{\xi}_{m,n}\rangle$ represents the local exciton state of the individual PIC molecule at $X^{\xi}_{m,n}$. This simple expression with the generalized coordinate is a direct consequence of the present form of the 1-D SG ($D_2{}^1$). However, we may have to appeal to such as cylindrical coordinates for an actual numerical evaluation of required quantities in the real systems for quantitative discussions.[43] The above equation is based on the assumption of the boundary condition to be applied, even for the incommensurate case of the 1-D crystal (if it is large enough).

4.2 Hamiltonian. Based on the above-defined local wavefunctions while considering the local symmetry of Fig. 2, the Hamiltonian for the molecular exciton state (with the operator representation) can be defined as

$$\begin{aligned} H = H_0 &+ V_1\sum_n\sum_m\{|A^{\alpha}_{m,n}\rangle\langle B^{\beta}_{m,n}| + |A^{\beta}_{m,n}\rangle\langle B^{\alpha}_{m,n}| \\ &+ |B^{\beta}_{m,n}\rangle\langle A^{\alpha}_{m,n}| + |B^{\alpha}_{m,n}\rangle\langle A^{\beta}_{m,n}|\} \\ &+ V_1'\sum_n\sum_m\{|A^{\alpha}_{m,n+1}\rangle\langle B^{\beta}_{m,n}| + |A^{\beta}_{m,n+1}\rangle\langle B^{\alpha}_{m,n}| \\ &+ |B^{\beta}_{m,n}\rangle\langle A^{\alpha}_{m,n+1}| + |B^{\alpha}_{m,n}\rangle\langle A^{\beta}_{m,n+1}|\} \\ &+ V_2{}^{\alpha}\sum_n\sum_m\{|A^{\alpha}_{m+1,n}\rangle\langle B^{\alpha}_{m,n}| + |B^{\alpha}_{m,n}\rangle\langle A^{\alpha}_{m+1,n}|\} \\ &+ V_2{}^{\beta}\sum_n\sum_m\{|A^{\beta}_{m,n}\rangle\langle B^{\beta}_{m,n}| + |B^{\beta}_{m,n}\rangle\langle A^{\beta}_{m,n}|\} + H', \end{aligned} \tag{3}$$

with $\{m\} = (1,2)$ and $\{n\} = (1,2,\ldots,N)$, subject to periodic boundary conditions. Here, H_0 is that for the free (dye) molecule, $X^{\xi}_{m,n}$; four kinds of V's stand for the matrix elements of excitation transfer between nearest neighbors[2] as indicated in Fig. 2. On the other hand, H' is that for the remaining (less significant) contributions, such as of its interaction with the surrounding solvent media, including the counter anion, whose effects may be dependent on the electronic states. Judging from the architecture made of the DL arrays (Section 2), we can safely set the (in-)equalities of

$$-V_1\ (\sim -V_1') > |V_2{}^{\alpha}(\sim V_2{}^{\beta})|, \tag{4}$$

e.g., by a numerical calculation based on a point-dipole approximation with a famous formula,[2]

$$\boldsymbol{V}_{i,j} = \boldsymbol{R}_{i,j}{}^{-3}\{\boldsymbol{M}_i\cdot\boldsymbol{M}_j - 3(\boldsymbol{R}_{i,j}\cdot\boldsymbol{M}_i)(\boldsymbol{R}_{i,j}\cdot\boldsymbol{M}_j)/R_{i,j}{}^{-2}\}. \tag{5}$$

Actually, the reduction of the site symmetry (section 3.1) did bring this predominance of the V_1 terms over the V_2 terms, contrary to the case of the primary octal helix, as mentioned in Section 2.

4.3 Symmetry-Adapted Wavefunctions. As evident in Fig. 2, the local symmetry group of the PIC molecule (to describe the symmetry of the PIC molecule including its environment) is C_1 at any site (with the approximate equivalence among sites, vide supra). Then, by creating (consulting) a character table for $D_2{}^1$ (whose subgroup is just D_2 PG), its irreducible representation (A only) is reduced to a combination of irreducible representations of the SG $D_2{}^1$, as

$$\chi^{l}_{A} = \chi^{s}_{A} + \chi^{s}_{B_1} + \chi^{s}_{B_2} + \chi^{s}_{B_3}. \tag{6}$$

Accordingly, $4\times 2 = 8$ sets of zeroth-order wavefunctions and energies, i.e. $\{|k\rangle^{\xi}_0(R)\}$ and $\{E^{\xi}_0(R)\}$, can be obtained, respectively, for the combination of the symmetry representations, $\{R\} = (A, B_1, B_2, B_3)$, and the stereomers, $\{\xi\} = (\alpha,\beta)$, without solving the secular equations concerning Eqs. 2, 3:

$$\begin{aligned} |k\rangle^{\xi}_0(A) = (4N)^{-1/2}\sum_n\{&|A^{\xi}_{1n}\rangle - |B^{\xi}_{1n}\rangle \\ &+ |A^{\xi}_{2n}\rangle - |B^{\xi}_{2n}\rangle\}\exp(ikbn), \end{aligned} \tag{7a}$$

$$E^{\xi}_0(A) = \Delta\mathcal{E} + D^{\xi}(A) - V_2{}^{\xi}; \tag{7b}$$

$$\begin{aligned} |k\rangle^{\xi}_0(B_1) = (4N)^{-1/2}\sum_n\{&|A^{\xi}_{1n}\rangle + |B^{\xi}_{1n}\rangle \\ &+ |A^{\xi}_{2n}\rangle + |A^{\beta}_{m,n}\rangle\}\exp(ikbn), \end{aligned} \tag{8a}$$

$$E^{\xi}_0(B_1) = \Delta\mathcal{E} + D^{\xi}(B_1) + V_2{}^{\xi}; \tag{8b}$$

$$\begin{aligned} |k\rangle^{\xi}_0(B_2) = (4N)^{-1/2} + \sum_n\{&|A^{\xi}_{1n}\rangle + |B^{\xi}_{1n}\rangle \\ &- |B^{\xi}_{1n}\rangle - |B^{\xi}_{2n}\rangle\}\exp(ikbn), \end{aligned} \tag{9a}$$

$$E^{\alpha(\beta)}_0(B_2) = \Delta\mathcal{E} + D^{\alpha(\beta)}(B_2) \mp V_2{}^{\alpha(\beta)}; \tag{9b}$$

$$\begin{aligned} |k\rangle^{\xi}_0(B_3) = (4N)^{-1/2}\sum_n\{&|A^{\xi}_{1n}\rangle - |B^{\xi}_{1n}\rangle \\ &- |A^{\xi}_{2n}\rangle + |B^{\xi}_{2n}\rangle\}\exp(ikbn), \end{aligned} \tag{10a}$$

$$E^{\alpha(\beta)}_0(B_3) = \Delta\mathcal{E} + D^{\alpha(\beta)}(B_3) \pm V_2{}^{\alpha(\beta)}. \tag{10b}$$

Here, $\Delta\mathcal{E}$ is the excitation energy of a free molecule. $D^{\xi}(R)$ is derived from the change in the interaction energy of one molecule with the others and the media accompanied with excitation. With an apparently equivalent contribution of the basis function, $|X^{\xi}_{m,n}\rangle$, to the wavefunctions (7a)–(10a) (excluding the sign $(+,-)$ and the phase factor $\exp(ikbn)$), the R dependence of $D^{\xi}(R)$ may not be very large, if we disregard the higher order terms through such as (intermolecular) charge-resonance states.[43]

4.4 Eigenfunctions and Eigenvalues. Applying the Hamiltonian (H) of Eq. 3 to the symmetry-adapted zeroth-order wavefunctions (for diagonalization) and making obvious definitions of

$$|k\rangle_{\pm}(R) \equiv 2^{-1/2}(|k\rangle_0^{\alpha}(R) \pm |k\rangle_0^{\beta}(R)) \tag{11a}$$

and

$$D(R) \equiv (D^{\alpha}(R) + D^{\beta}(R))/2, \tag{11b}$$

the eigenfunctions $\{|k\rangle_{\pm}(R)\}$ and eigenvalues $\{E_k^{\pm}(R)\}$ (both approximate but adequate, especially within the point-dipole approximation) can easily be obtained, as follows:

$$\begin{aligned}|k\rangle_{\pm}(A) = (8N)^{-1/2} \sum_n \| &|A_{1n}^{\alpha}\rangle \pm |B_{1n}^{\beta}\rangle \mp |A_{1n}^{\beta}\rangle - |B_{1n}^{\alpha}\rangle \\ &+ |A_{2n}^{\alpha}\rangle \pm |B_{2n}^{\beta}\rangle \mp |A_{2n}^{\beta}\rangle \\ &- |B_{2n}^{\alpha}\rangle\} \exp(ikbn),\end{aligned} \tag{12a}$$

$$\begin{aligned}E_k^{\pm}(A) = \Delta\mathcal{E} + D(A) \pm V_1 \pm V_1' \cos(kb) \\ - (V_2^{\alpha} + V_2^{\beta})/2;\end{aligned} \tag{12b}$$

$$\begin{aligned}|k\rangle_{\pm}(B_1) = (8N)^{-1/2} \sum_n \{&|A_{1n}^{\alpha}\rangle \pm |B_{1n}^{\beta}\rangle \pm |A_{1n}^{\beta}\rangle + |B_{1n}^{\alpha}\rangle \\ &+ |A_{2n}^{\alpha}\rangle \pm |B_{2n}^{\beta}\rangle \pm |A_{2n}^{\beta}\rangle \\ &+ |B_{2n}^{\alpha}\rangle\} \exp(ikbn),\end{aligned} \tag{13a}$$

$$\begin{aligned}E_k^{\pm}(B_1) = \Delta\mathcal{E} + D(B_1) \pm V_1 \pm V_1' \cos(kb) \\ + (V_2^{\alpha} + V_2^{\beta})/2;\end{aligned} \tag{13b}$$

$$\begin{aligned}|k\rangle_{\pm}(B_2) = (8N)^{-1/2} \sum_n \{&|A_{1n}^{\alpha}\rangle \pm |B_{1n}^{\beta}\rangle \pm |A_{1n}^{\beta}\rangle + |B_{1n}^{\alpha}\rangle \\ &- |A_{2n}^{\alpha}\rangle \mp |B_{2n}^{\beta}\rangle \mp |A_{2n}^{\beta}\rangle \\ &- |B_{2n}^{\alpha}\rangle\} \exp(ikbn),\end{aligned} \tag{14a}$$

$$\begin{aligned}E_k^{\pm}(B_2) = \Delta\mathcal{E} + D(B_2) \pm V_1 \pm V_1' \cos(kb) \\ - (V_2^{\alpha} - V_2^{\beta})/2;\end{aligned} \tag{14b}$$

$$\begin{aligned}|k\rangle_{\pm}(B_3) = (8N)^{-1/2} \sum_n \{&|A_{1n}^{\alpha}\rangle \pm |B_{1n}^{\beta}\rangle \mp |A_{1n}^{\beta}\rangle - |B_{1n}^{\alpha}\rangle \\ &- |A_{2n}^{\alpha}\rangle \mp |B_{2n}^{\beta}\rangle \pm |A_{2n}^{\beta}\rangle \\ &+ |B_{2n}^{\alpha}\rangle\} \exp(ikbn),\end{aligned} \tag{15a}$$

$$\begin{aligned}E_k^{\pm}(B_3) = \Delta\mathcal{E} + D(B_3) \pm V_1 \pm V_1' \cos(kb) \\ + (V_2^{\alpha} - V_2^{\beta})/2.\end{aligned} \tag{15b}$$

If we disregard the R (i.e., $X_{m,n}^{\xi}$) dependence on $D(R)$ and assume the near equality of $V_2^{\alpha} \approx V_2^{\beta}$ (instead of $V_2^{\alpha} \sim V_2^{\beta}$) as perhaps being nearly equivalent to invoking the point-dipole approximation, Eqs. 14,15 are accidentally degenerate. With inequality (4) and the relationship $0 \leq 1 + \cos(kb) \leq 2$, these four energy bands are significantly overlapped, but barely separated into two sets of bands corresponding to the sign ($\pm$) for each symmetry, R.

4.5 Assignments of the (Polarized) Absorption Spectra. The exciton states are obtained as above. Therefore, for assigning the absorption band with the polarization, the actual transition moments to these states from the ground state have to be evaluated. For that purpose,

(1) the transition moment ($\boldsymbol{M}$) in each PIC molecule is separated into x, y, and z components with

$$\begin{aligned}&\boldsymbol{M}_x = \boldsymbol{M}\cos\gamma\cos\theta_{m,n}, \boldsymbol{M}_y = \boldsymbol{M}\cos\gamma\sin\theta_{m,n}, \\ &\boldsymbol{M}_z = \boldsymbol{M}\sin\gamma; \theta_{m,n} \approx \theta_{0,0} + \pi m + (\pi/2)_n.\end{aligned} \tag{16}$$

Here, $\theta_{0,0}$ (the only parameter taken from the cylindrical coordinates) is dependent on the actual choice of the $x(y)$ axis. However, for evaluating the n-dependent sum (i.e., that on m) in the transition moments, a common procedure of a simple pictorial vector sum can be taken within each disk. Furthermore, two more prescriptions are available to find nonzero transition moments:

(2) Group theory may be regarded to be a golden rule to find an allowed/forbidden transition. Thus, just by inspecting the (created) character table for the $D_2{}^{(1)}$ symmetry, two kinds of allowed transitions with polarizations of $B_1 \parallel z$ and $(B_2, B_3) \perp z$, respectively, are found as well as the forbiddeness of the transition to the A state.

(3) The $-$ states in the Eqs. 12a–15a are observed to be practically forbidden by cancellation in the vector sum corresponding to the constituent $\{|A_{mn}^{\xi}\rangle - |B_{mn}^{\xi'}\rangle\}$ with $\xi \neq \xi'$ in the eigenfunction, as may be termed parity forbidden (forbidden within the point-dipole approximation). These molecules are related by the approximate C_2 operation (not symbol-marked with the filled lens-shape in Fig. 2).

(4) As for the k dependence, it has to be recalled that it is defined complementary to b or n, i.e. not for a simple translation (b as spread), but related to a screw operation consisting of an approximate $C_4(z)^n$ operation. Therefore, it brings a direct influence on the transition moment, i.e. on the polarization, as implied by Eq. 16.

(5) Since this system is a (1-D) crystal where phonons with the total (linear quasi-) momentum, i.e. K_{p} and $K_{\mathrm{p}}{}^0$ (in unit of $\hbar$) for the exciton state(s) and the ground states, respectively, are possibly involved, a conservation law for the total momentum of the entire system (including that of the electromagnetic field) has to be considered with a (simplified) relationship,

$$K_{\mathrm{t}}{}^{\parallel} = k\sin\gamma + K_{\mathrm{p}} = K_{\mathrm{p}}{}^0 + k_{\mathrm{p}}{}^{\parallel}, \tag{17a}$$

where k and $k_{\mathrm{p}}{}^{\parallel}$ are those for the exciton state (as already defined in Eqs. 2) and for the incident photon (its z component), respectively, with the available magnitudes,[43]

$$|k_{\mathrm{p}}{}^{\parallel}| \leq |k_{\mathrm{p}}| = 2\pi/\lambda_{\mathrm{p}} \ll \pi/b; |k| \leq \pi/b; |K_{\mathrm{p}}^{(0)}| \sim \pi/b. \tag{17b}$$

Therefore, in addition to the above four kinds of factors, the relationship

$$k\sin\gamma \approx K_{\mathrm{p}}{}^0 - K_{\mathrm{p}} \equiv \Delta K_{\mathrm{p}} \tag{17a'}$$

must be satisfied.

Thus, the following three states only are evaluated to be allowed at the zeroth order, as extracted from Eqs. 12–15, besides the corresponding energies (with some distributions for the latter two):

$$|0\rangle_+(B_1) \parallel z,$$

$$E_0^+(B_1) = \Delta\mathcal{E} + D(B_1) + V_1 + V_1' + (V_2{}^\alpha + V_2{}^\beta)/2; \quad (18)$$

$$|k \approx (\pi/2)/b\rangle_+(B_2) \perp z,$$

$$E^+_{k\approx(\pi/2)/b}(B_2) \approx \Delta\mathcal{E} + D(B_2) + V_1 - (V_2{}^\alpha - V_2{}^\beta)/2; \quad (19)$$

$$|k \approx (\pi/2)/b\rangle_+(B_3) \perp z,$$

$$E^+_{k\approx(\pi/2)/b}(B_3) \approx \Delta\mathcal{E} + D(B_3) + V_1 + (V_2{}^\alpha - V_2{}^\beta)/2. \quad (20)$$

The restriction to $k = 0$ in Eq. 18 is just based on the assumption of little involvement of the phonon mode for the present system at (below) room temperature (as is consistent with the observed sharp J band). While the restriction to $k \approx (\pi/2)/b$ in the last two equations (as made for the vector sum (on n) to be out-of-cancellation) corresponds to the approximate $C_4(z)$ operation in the screw operation. (While, $k \approx -(\pi/2)/b$ for the enantiomer of what is described by Fig. 2.) Now, the Davydov splitting is clearly exhibited, which consists of one sharp $\parallel$ J and two broad $\perp$ H bands (all fundamentals, no progression being assumed as a common conduct for the large aggregates, with the focused Franck-Condon factors at the 0,0 bands), where the B_1 state is located lower than the B_2 and B_3 states by as much as 500–3000 cm^{-1} by applying Eq. 4 ($\sim -V_1'$, with strong dependence on the geometry and about consistent with the previously assumed values[15,17,25,28]) close to the observed value of $\sim$2300 cm^{-1}, with the ratio of their integrated intensities being ca. 1:1.3 corresponding to $\gamma \approx 38^\circ$ ($\tan 52^\circ \approx 1.3$), nearly reproducing the observed ratio of ca. 1:1.5. (In actuality, as implied in Introduction with Fig. 1, this value itself (as was determined from the observed spectra) is also a subject for a critical examination in a coming paper.[43]) The reasons for the broad H bands are: (1) Near equality of $k \approx (\pi/2)/b$ due to the discrete nature of the values of $k_\nu = (2\pi/Nb)\nu$ with $-N/2 < \nu \leq N/2$ for a finite N value, as defined in Eq. 2b (not always consistent with the assumption of a periodic boundary condition), causing intensity distribution among several k levels within the band. (2) Distributed finite N numbers i.e., sizes of the J aggregates. (The exact equality, i.e. $k = (\pi/2)/b$ (with $\nu = N/4$) is satisfied only when N is accidentally a multiple of 4.) (3) Contribution of the photon modes as critically required by Eq. 17a′ with various combinations of $\{\Delta K_p\}$. Here, it should also be noted that a criterion for the strong appearance of the H bands is not simply the formation of a H-type arrangement to give rise to H-type exciton states (like in crystals with "large" V_2 values: It is indeed rolled, in the present model, with the smaller V_2 values than the V_1 values.), but rather due to the small angle, γ, made while winding the DL arrays into a pillar. Though the two transitions corresponding to Eqs. 19, 20 with an energy separation of $D(B_2) - D(B_3) - (V_2{}^\alpha - V_2{}^\beta)$ between them might be regarded as accidentally degenerate, while carrying equal intensities based on Eq. 16 (corresponding to the cylindrical symmetry, under the point-dipole approximation, i.e. disregarding chirality of PIC molecules), their degeneracy/equivalence can be easily removed by modifying the geometry towards lower (site) symmetry, e.g. by modifying the cylinder into a twisted elliptic form (like a twisted electric cord with an elliptic/flat cross section, as may be one of the best models if Fig. 1 is to be interpreted by a unique helix structure; thus with a more complex version of Eq. 16) and/or by taking account of the contribution of the higher-order terms on the above values, as will be discussed in future.[2,3,43] (In view of the geometry, two PIC enantiomers are no longer equivalent physically if they are wound on the pillar. This may indicate one of the limitations of employing the spread/projected view for the 1-D crystal as a common procedure, two sides not being equivalent.) In this way, the observed polarization spectra, e.g. with an energy separation of $\sim$1500 cm^{-1} for the double H bands, are well interpreted, at least in semi-quantitative manner. Though the observed energy separation can easily be reproduced by adjusting the parameters in $D(B_2) - D(B_3) - (V_2{}^\alpha - V_2{}^\beta)$ (too many, in contrast to the cases of Refs. 17, 18, 33, and 34), it will not be realistic unless an actual modification of the structure is made into those with lower (site) symmetries.[43] Thus, even at this level of description, no scheme of intensity mixing is required to produce the double H bands, e.g. by invoking vibronic coupling through a nonadiabaticity operator.[15,17]

The corresponding parity-forbidden components are as follows:

$$|0\rangle_-(B_1) \parallel z,$$

$$E_0^-(B_1) = \Delta\mathcal{E} + D(B_1) - (V_1 + V_1') + (V_2{}^\alpha + V_2{}^\beta)/2; \quad (18')$$

$$|k \approx (\pi/2)/b\rangle_-(B_2) \perp z,$$

$$E^-_{k\approx(\pi/2)/b}(B_2) \approx \Delta\mathcal{E} + D(B_2) - V_1 - (V_2{}^\alpha - V_2{}^\beta)/2; \quad (19')$$

$$|k \approx (\pi/2)/b\rangle_-(B_3) \perp z,$$

$$E^-_{k\approx(\pi/2)/b}(B_3) \approx \Delta\mathcal{E} + D(B_3) - V_1 + (V_2{}^\alpha - V_2{}^\beta)/2. \quad (20')$$

All of these are expected to show weak absorption bands at shorter wavelengths than those of the H bands with energy shifts of as much as $\sim -2V_1$ or more (>1000 cm^{-1}), i.e. near the valley of the entire bands corresponding to the $S_1 \leftarrow S_0$ and $S_2 \leftarrow S_0$ transitions of the monomer. However, they are not evident in the observed polarization spectra, endorsing the parity forbiddeness.

4.6 Assignments of CD Spectra. This section is aimed at modifying the existing theory of optical rotation,[3–5] so that it can be applied to a general 1-D crystal, including the present PIC J aggregates. However, verification is made only for the helix with 4 DL arrays, according to the constitution of this Section.

Optical rotation is a combination of electronic and magnetic transitions, as expressed by the rotational strength (with the assumption that the size/length of the aggregate is much less than the wavelength of the incident light, corresponding to $N \sim (<)100$ of mesoscopic size),

$$\boldsymbol{R}_{a0} = \mathbf{I}\mathrm{m}\{<0|\boldsymbol{M}|a><a|\boldsymbol{m}|0>\}, \quad (21)$$

where a represents an excited state of concern, i.e. $|k\rangle_\pm(R)$, as

expressed by Eqs. 12–15 in the case of the present PIC J aggregates, while $\boldsymbol{M}$ and $\boldsymbol{m}$ are for electronic and magnetic transition moment operators, respectively. In the case of the PIC J aggregates whose excited states can be approximately represented as Frenkel-type exciton states, as described above, it can be further reduced to

$$R_k^{\pm}(R) = \mathbf{I}\mathrm{m}\Bigg[(\pi E_k^{\pm}(R)i/hc)\sum_i\sum_j c_{i,k}^{\pm}(R)c_{j,k}^{\pm *}(R) \times \boldsymbol{R}_j\cdot(\boldsymbol{M}_j\times\boldsymbol{M}_i)\Bigg] \tag{22}$$

with $\{i, j\} = \{X_{m,n}^{\xi}\}$, while $c_{i,k}^{\pm}(R)$ is an expansion coefficient for the corresponding wavefunction $|k\rangle_{\pm}(R)$ at molecule i. The vector $\boldsymbol{M}_i$ is a matrix element of the (electronic) transition dipole moment operator $\boldsymbol{M}$ at i. On the other hand, $\boldsymbol{R}_j$ is a position vector of molecule j to be measured from an origin, set arbitrary in the aggregate. Since $c_{i,k}(R)$ is a complex number including a factor exp($ikbn$), more discussion is required to evaluate Eq. 22.

Now, let's turn to the interpretation of the observed CD spectra. If we restrict it to the resonance case, i.e. to the area of optical absorption, the calculation of Eq. 22 is reduced only to three cases corresponding to Eqs. 18–20 with $k = 0$ or $\approx (\pi/2)/b$. (Recall the original definition with Eq. 21.) Thus, just taking a look at the wavefunctions for these cases, the coefficients with a factor exp($ikbn$) are found to be either real for $k = 0$ with any n and for $k \approx (\pi/2)/b$ with even n or pure imaginary for $k \approx (\pi/2)/b$ with odd n, respectively. Therefore, an equality of $c_i c_j^* = c_j c_i^*$ is derived for the pair (i, j) with $\Delta n = 0$, i.e. within the unit cell. Furthermore, we now introduce a nearest-neighbor approximation to restrict the summation in Eq. 22. Thus, by a careful examination of the wavefunctions, Eqs. 19,20, while consulting Eqs. 14a,15a, the common equality of $c_i c_j^* = c_j c_i^*$ is verified for any adjacent pair (i, j). With this equality and using the formula of vector products, the following rearrangement can be made for the pair:

$$\begin{aligned} &c_i c_j^* \boldsymbol{R}_j\cdot(\boldsymbol{M}_j\times\boldsymbol{M}_i) + c_j c_i^* \boldsymbol{R}_i\cdot(\boldsymbol{M}_i\times\boldsymbol{M}_j) \\ &= c_i c_j^* (\boldsymbol{R}_j - \boldsymbol{R}_i)\cdot(\boldsymbol{M}_j\times\boldsymbol{M}_i) \\ &\equiv c_i c_j^* \boldsymbol{R}_{j,i}\cdot(\boldsymbol{M}_j\times\boldsymbol{M}_i). \end{aligned} \tag{23}$$

Therefore, Eq. 22 is further simplified to

$$R_k^{+}(R) = \mathbf{I}\mathrm{m}[(\pi E_k^{+}(R)i/hc)\sum_{(i,j)} c_{i,k}^{+}(R) \times c_{j,k}^{+*}(R)\boldsymbol{R}_{j,i}\cdot(\boldsymbol{M}_j\times\boldsymbol{M}_i)] \tag{24}$$

with $k = 0$ and $\approx (\pi/2)/b$ for the plus states (so parity restricted) and with the symmetries $R = B_1$ and B_2 and B_3, respectively, where summation should be taken for the adjacent pairs of (i, j). Thence, the quantity in the sum is recognized to be just concerned within each pair (independent of the coordinate system). Namely, the sum rule of the rotational strength on the pair is now established for the present system of Fig. 2, (as a matter of course) as had been proven for the system with a finite number of chromophores (Section 10.8 of Ref. 5). This conclusion should also be extended to any helices, including those subject to incommensurate screw operations, just by applying mathematical techniques to take for limits, e.g. most conventionally, by assuming periodic boundary conditions.[2,3,43] By taking account of the local symmetry, as illustrated by Fig. 2, only four kinds of triple products, $\{\boldsymbol{R}_{j,i}\cdot(\boldsymbol{M}_j\times\boldsymbol{M}_i)\}$, are to be evaluated that may be termed R_1, R_1', R_2^{α}, and R_2^{β}, just made correspondent to the V's in the Hamiltonian of Eq. 3. As will be described in future,[43] these triple products can be estimated under the point-dipole approximation by expressing the concerned vectors in terms of cylindrical coordinates. Although the actual values are heavily dependent on the geometry, the sign of the above R values are all confirmed to be negative for any possible geometries of the enantiomer of the helix structure, as illustrated in the Fig. 2. Thus, the relationship

$$-R_0^{+}(B_1) > R_{k\approx(\pi/2)/b}^{+}(B_2) \sim R_{k\approx(\pi/2)/b}^{+}(B_3) > 0 \tag{25}$$

is confirmed by examining Eq. 24 with Eqs. 18–20. This result is just consistent with the observed CD spectra with opposite signs between the J and H bands.[9,12,14]

5. Concluding Remarks

As described above, all of the three peculiarities could be interpreted by the present model, most typically with Eqs. 18–20, 25, thus demonstrating the advantage of this model over any others so far proposed. Furthermore, the importance of hydrophobic groups and the indication of the 8-membered core are other facts interpreted anew by the present model (vide supra). In a succeeding publication,[43] the other experimental data, such as X-ray diffraction data[8] will be interpreted by refinement of the model, i.e. by modifications of the geometries of the J aggregates, while evaluating such parameters as $\{V\}$ and $\{R\}$. For example, to interpret the coincidence of the observed lattice constant (for PIC-F) with $2b$ of the present model (Section 2), the apparent/effective size of the unit lattice (to say precisely, the primitive lattice of the DL array) has to be expanded twice by a modification (further reduction?) of the site symmetry, e.g. by assuming an alternating structure, such as a $(\alpha\alpha\beta\beta)_{N/2}$ type, in the DL array in place of the $(\alpha\beta)_N$ type. Figure 3 shows a structure that meets this requirement, as made contrast to that in Fig. 2 (presumed for PIC-Cl). In spite of the significant change in the shape of the primitive lattice ($\gamma \approx 90^\circ$ now, in spite of the minor change of the tilt angle of the DL array), the mutual arrangement of the constituent molecules in the unit cell is not very different from that in Fig. 2. In accordance to this change in the structure, the whole formalism in Section 4 with such as Eqs. 2–25 has to be modified. Nevertheless, little significant change is seen in the interpretation of the experimental data, such as the absorption spectra (including the failure to interpret the broad $\|$ band), except for the lattice constant.[43] Up to this stage, to show a photograph of a unit cell composed of molecular models (Fig. 4, as a transitory structure with tentative location of Cl^- ions) may be adequate to help the reader to imagine what is meant by Figs. 2 and 3, more precisely. Though this was originally prepared to show the structure of PIC-Cl, it hap-

Fig. 4. An example of a unit cell of the helical PIC-Cl J aggregates prepared with molecular models whose constituent atoms are sized with van-der-Waals radii and colored with black (C), transparent (H), blue (N), and green (Cl^-). Due to a technical difficulty, the glass-made holder (with a complex inner-structure) could not be the same as that which was designed with sheets of cardboard and a lump of synthetic clay. This fact under the influence of gravity is the main cause for the discrepancy (e.g., with tilt angle of $\sim 45^\circ$), as described in the text, inhibiting the formation of the tightest possible structure.

pened to be rather close to Fig. 3 for PIC-F. This fact may be taken being an evidence of the feasibility of a structural variation in the J aggregate. The contributions of the PIC octamer(s), 12-mer(s), 16-mers, or other, and of the variations of the helices even including those with 6 DL arrays of the ${D_3}^1$ symmetry, are to be considered as well, which are supposed to be involved in the course of the aggregation processes. Notwithstanding the exact degeneracy involved in the system with the ${D_3}^1$ symmetry (the case of 12-mer in the unit cell), practically the same conclusion as in the ${D_2}^1$ case will be derived, with the major difference being a smaller γ ($\approx 30^\circ$).[43] Therefore, the effects of the contribution of this conformer in the solution at room temperature are presumed to be (1) a larger intensity ratio (H/J) and (2) broader absorption bands.

As introduced, a complete interpretation of the individual facts, as described in Sections 1 and 2, is also left for later discussion,[43] though some of them are almost obvious, at least qualitatively: (1) The initial step of aggregation can be interpreted as being due to the involvement of the cyclic octamer (or 12-mer), postulated as a core toward the formation of the J aggregate, instead of the dimer/tetramer,[11,12,15] of which no J band is predicted to correspond to the extreme case of $N = 1$, i.e. of $\nu = k = 0$ and $V_1' = 0$ in Section 4. The two bands of the "dimer", as simulated in Ref. 15, are rather ascribed to such as an octamer, for the other $\{V\}$ values need not exactly coincide with those in the J aggregate. (2) A gradual change is noted in the spectral shape through progress of association, i.e. with growth of aggregates. (3) The helix cannot be formed in the monolayer, as a matter of course. (4) Long pillar of aggregates formed in the fluid solution could be destroyed into smaller pieces of clusters in a rigid media (at low temperature). (5) The larger is the ionic radius of the counter halide ion, the larger is the contribution of the helix that consists of 6 DL arrays (as is confirmed with molecular models). Actually, the DL array in this helix with more ellipticity appears to have a tighter structure with a larger helix diameter and a smaller value of γ, i.e. with a more predominant $\{-V_1\}$ value over $\{|V_2|\}$ (cf. Eq. 4) than that in a slender helix, resulting in a greater population of the red conformer with a higher intensity of H bands. This appears to be consistent with the observation of two kinds of aggregates, as described in the second last paragraph of section 1.2. However, another interpretation is also possible as due to possibility of two kinds of the DL arrays (in the helices; Fig. 2 vs Fig. 3) as just described in the preceding paragraph.[43]

In addition to what is listed above, significant changes in the fine details are predicted, such as the appearance of another $\| z$ absorption band (Fig. 1; stronger than the parity-forbidden B_1 component at the shorter wavelength region (Eq. 18′), by a slight deformation of the structure (to ${C_2}^1$, as an extreme example) due to an irregularity in the DL array, a breakdown of the periodic boundary condition, and/or other higher order contributions (section 4.5). Though not so obvious, these can interpret the H/J ratio more quantitatively by allowing for mixing between the A and B_1 states, consistent with the observed complex/scrambled polarization spectra. What is aimed at as a final goal is, of course, a search for the true geometries, probably with lower symmetries either in SG or in the unit cell, in addition to a minor change in geometry, e.g. by allowing for the average molecular plane to be nonvertical to the cylinder (no longer parallel to each other in the spread view) for better contact between the π planes. This has to be done while evaluating various quantities, as required (vide supra) and even by taking account of such as (pseudo-) Jahn-Teller effect. All of these appear to have complex dependencies on the counter anions. Thus, there are many combinations of conformers to choose (as modifications of those shown as Figs. 2 and 3) for interpreting the experimental data. A discussion of the peculiarity of the PIC J aggregate, as compared to other typical J aggregates, such as of TDBC and ICG, may also be helpful.[31,48–51] Actually, for the case of prototypical and nonpeculiar TDBC, extremely weak (H ?) bands is observed in the blue region of the tail of the J band in addition to the evidence of its octamer.[48] This can be interpreted by the difference in the structures between the PIC and TDBC J aggregates. The latter may have the appearance of a revolving door consisting of 4 DL arrays with the highest possible (local) symmetry of ${D_2}^1$ (with a symmetry operation, i.e. screw operation $\{C_4|\tau\}$ whose square is $\{C_2|t_1\}$, as described by the Seitz operators[45]). While in another representative case of ICG, the formation of a dimer (with the shape of the engaged C characters[43]) satisfying a mass reaction law is clearly verified,[50] in contrast to the case of PIC and TDBC. In both typical systems (with the SO_3^- groups), a modified version of Eq. 1b is actually applied while replacing M^+ and X^- with M^- and Na^+, respectively. An interpretation of recent experimental data on the PIC J aggregate will be made as well, such

as (1) at a mica/water interface[35] and (2) with a reflection microscopy of spin-coated samples.[36]

References

1 Presented at Symposium on Molecular Structure held at Tokyo in September 2000, 3p129, p. 735.

2 A. S. Davydov, ''Theory of Molecular Excitons,'' Plenum, New York (1971).

3 M. R. Philpott, *Adv. Chem. Phys.*, **23**, 227 (1973).

4 I. Tinoco, R. W. Woody, and D. F. Bradley, *J. Chem. Phys.*, **38**, 1317 (1963).

5 N. Harada and K. Nakanishi, ''Circular Dichroic Spectroscopy: Exciton Coupling in Organic Stereochemistry,'' University Science Books, Mill Valley (CA) (1983).

6 G. Scheibe, *Angew. Chem.*, **50**, 212 (1937).

7 E. E. Jelly, *Nature (London)*, **139**, 631 (1937).

8 W. Hoppe, *Kolloid-Z.*, **109**, 27 (1944).

9 S. F. Mason, *Proc. Chem. Soc.*, **1964**, 119.

10 G. Scheibe, ''Lage, Intensität und Structur von Absorptionbanden, in: Optische Angerungen organischer Systeme,'' ed by W. Foerst, Verlag Chemie, Wienheim (1966), p. 109.

11 W. Cooper, *Chem. Phys. Lett.*, **7**, 73 (1970).

12 E. Daltrozzo, G. Scheibe, K. Gschwind, and F. Haimerl, *Photogr. Sci. Eng.*, **18**, 441 (1974).

13 H. J. Nolte, *Chem. Phys. Lett.*, **31**, 134 (1975).

14 B. Nordén, *J. Phys. Chem.*, **81**, 151 (1977).

15 B. Kopainsky, J. K. Hallermeier, and W. Kaiser, *Chem. Phys. Lett.*, **83**, 498 (1981).

16 B. Kopainsky, J. K. Hallermeier, and W. Kaiser, *Chem. Phys. Lett.*, **87**, 7 (1982).

17 P. O. J. Scherer and S. F. Fischer, *Chem. Phys.*, **86**, 269 (1984).

18 E. W. Knapp, P. O. J. Scherer, and S. F. Fischer, *Chem. Phys. Lett.*, **111**, 481 (1984).

19 H. Gruhl, H.-P. Dorn, and K. Winzer, *Appl. Phys.*, **B38**, 199 (1985).

20 C. Duschl, D. Kemper, W. Frey, P. Meller, H. Ringsdorf, and W. Knoll, *J. Phys. Chem.*, **93**, 4587 (1989).

21 F.-J. Schmitt and W. Knoll, *Chem. Phys. Lett.*, **165**, 54 (1990).

22 R. Hirschmann, W. Köhler, J. Friedrich, and E. Daltrozzo, *Chem. Phys. Lett.*, **151**, 60 (1988).

23 H. Wendt and J. Friedrich, *Chem. Phys.*, **210**, 101 (1996).

24 H. Fidder, J. Terpstra, and D. A. Wiersma, *J. Chem. Phys.*, **94**, 6895 (1991).

25 N. Kanamaru, Presented at Symposium on Molecular Structure held at Tokyo in September 1994, 2P64, p. 337.

26 K. Misawa, S. Machida, K. Horie, and T. Kobayashi, *Chem. Phys. Lett.*, **240**, 210 (1995).

27 ''J-Aggregates,'' ed by T. Kobayashi, World Scientific, Singapore (1996).

28 H. Kuhn and C. Kuhn, in Ref. 27, pp. 1–40.

29 K. Misawa and T. Kobayashi, in Ref. 27, pp. 41–65.

30 P. O. J. Scherer, in Ref. 27, pp. 95–110.

31 M. Lindrum and I. Y. Chan, *J. Chem. Phys.*, **104**, 5359 (1996).

32 I. Renge and U. P. Wild, *J. Phys. Chem. A*, **101**, 7977 (1997).

33 T. Kato, F. Sasaki, S. Abe, and S. Kobayashi, *Chem. Phys.*, **230**, 209 (1998).

34 T. Kato, F. Sasaki, and S. Kobayashi, *Chem. Phys. Lett.*, **303**, 649 (1999).

35 H. Yao, S. Sugiyama, R. Kawabata, H. Ikeda, O. Matsuoka, S. Yamamoto, and N. Kitamura, *J. Phys. Chem. B*, **103**, 4452 (1999).

36 M. Vacha, M. Saeki, O. Isobe, K. Hashizume, and T. Tani, *J. Chem. Phys.*, **115**, 4973 (2001).

37 B. Neumann, *J. Phys. Chem. B*, **105**, 8268 (2001).

38 N. Fukutake and T. Kobayashi, *Chem. Phys. Lett.*, **356**, 368 (2002).

39 A. Eisfeld and J. S. Briggs, *Chem. Phys.*, **281**, 61 (2002).

40 K. Nakatsu, H. Yoshioka, and H. Morishita, *Acta Cryst.*, **B33**, 2181 (1977).

41 B. Dammeier and W. Hoppe, *Acta Crystallogr., Sect. B*, **27**, 2364 (1971).

42 D. L. Smith, *Photogr. Sci. Eng.*, **18**, 309 (1974).

43 N. Kanamaru, to be published later.

44 ''International Tables for Crystallography,'' ed by T. Hahn, D. Reidel Pub., Boston (1987).

45 G. Burns and A. M. Glazer, ''Space Groups for Solid State Scientists'' 2nd ed, Academic Press, Boston (1990).

46 A. V. Shubnikov and V. A. Koptsik, ''Symmetry in Science and Art,'' Plenum, New York (1974), Chap. 6, Symmetry of Rods.

47 B. K. Vainshtein, ''Modern Crystallography 1, Fundamentals of Crystals (2nd Ed.)'', Springer, Berlin (1994), sect. 2.7.3, Cylindrical (Helical) Groups $G_1{}^3$.

48 S. Makio, N. Kanamaru, and J. Tanaka, *Bull. Chem. Soc. Jpn.*, **53**, 3120 (1980).

49 U. DeRossi, S. Dähne, S. C. J. Meskers, and H. P. J. M. Dekkers, *Angew. Chem., Int. Ed. Engl.*, **35**, 760 (1996).

50 M. Mauerer, A. Penzkofer, and J. Zweck, *J. Photochem. Photobiol. B: Biol.*, **47**, 68 (1998).

51 J. Zweck and A. Penzkofer, *Chem. Phys.*, **269**, 399 (2001).